JOURNAL OF MATERIALS SCIENCE **38** (2003) 891–900

Combined modelling and experimental studies of rubber toughening in polymers

J. P. DEAR
Department of Mechanical Engineering, Imperial College of Science, Technology and Medicine, Exhibition Road, London SW7 2BX, UK
E-mail: j.dear@ic.ac.uk

When researching the effect of rubber toughening in acrylonitrile-butadiene-styrene (ABS) copolymer and high-impact polystyrene (HIPS) and also toughening methods used in other materials, then, often comparisons are needed between materials with and without the toughening agents over the full crack velocity range. This is from the threshold stress to just maintain crack propagation up to the limiting crack velocity conditions. However, the toughening of materials can change other material properties including, for example, the onset of yield in the material under static stress. The result can be that a crack velocity versus stress curve cannot be obtained by experiment over the full crack velocity range for some toughened materials. However, as used in this study, combined experimental and computer simulations can provide for a meaningful and informative comparison between crack velocity versus stress curves for materials with and without toughening agents over the full crack velocity range.

1. Introduction

For many uses of materials in stressed structures and components, key requirements of the materials are often low density, high stiffness and good toughness. Many polymers and polymer composites can satisfy the first two requirements and a great deal of research has been devoted to improving their toughness [1–4]. This is with the aim of minimising the effect on the material's weight and stiffness when introducing toughening agents or other means of increasing the material's resistance to crack propagation. In this study, two polymers have been researched as to the effect on the material about the crack tip of using rubber particles as the toughening agent. One of these materials is acrylonitrile-butadiene-styrene (ABS) copolymer and the other is high-impact polystyrene (HIPS). The effect of using rubber particles in these two materials is different [5–8]. For ABS, the rubber particles tend to produce more yielding about and ahead of the crack tip whilst for HIPS, there is a greater tendency to promote more crazing in the host material around the rubber particles. In this study, the toughness improvement produced by the use of rubber particles in the two materials, ABS and HIPS, is compared with styrene-acrylonitrile (SAN) host matrix and the polystyrene (PS) host matrix respectively. This is for the full crack velocity range from the stress level to just maintain crack propagation up to the limiting crack velocity condition. For toughened polymers, it can be difficult by experiment, to achieve experimental data over the required full crack velocity range. This is because of the earlier onset of static yielding (or crazing) in the toughened material. The lower static yield stress of ABS and the lower craze stress of HIPS (compared with SAN and PS) means the experimental crack velocity versus stress curves can only be obtained at lower crack velocities. In this research, combined experimental studies and dynamic modelling are employed when necessary to generate full crack velocity versus stress curves that relate only to the toughening effects at the crack tip. This is so that, for this study, the crack velocity versus stress effects can be compared before and after the host material is toughened over the full crack velocity range that relate to toughening effects at the crack tip.

With the much-increased power of personal computer (PC) size of machines that are now frequently used to capture experimental data, it is possible to host a dynamic model on the same PC machine. This is very convenient, as in this and similar studies, many experiments and modelling simulations are needed. For the modelling used, to simulate the build up and dynamic transfer of strain energy to the tip of a propagating crack, a distributed mass-spring network is employed. The distributed mass-spring network has been devised so that the simulated material's Young's modulus, Poisson's ratio and damping can be varied. Also, the conditions around the crack tip can be dynamically varied for the different toughness and response rate of the simulated materials. A big advantage of the modelling arrangement devised is that it can be programmed and provide the required different simulation data quickly so that it is promptly available for comparison with experimental data that are being processed on the same PC machine.

For this and many other fracture studies often required is crack propagation in small specimens of

material when the only strain energy available to the crack tip is that precisely stored in the material in a stress relaxed state. To achieve this in a small specimen requires a crack initiation technique that does not disturb the evenly distributed strain energy stored in the material in its prepared stress relaxed state. The crack initiation technique used in this study is the frozen tongue method [9, 10]. A crack is initiated in the frozen tongue section and when it enters the main section of the specimen it quickly achieves constant velocity crack propagation in a short distance. The subsequent crack velocity then only relates to the strain energy stored in the specimen prior to crack initiation and the dimensions of the specimen if these dimensions limit the dynamic strain energy available to the crack tip. In this study, the specimens were appropriately small but were of sufficient dimension to provide for the attachment of instrumentation sensors to monitor the crack velocity. Also, the crack path was sufficiently long to achieve good and consistent fracture surfaces. This is from the threshold to just maintain crack propagation up to the limiting crack velocity conditions.

The PC modelling used was devised to simulate the same crack velocity versus stress data that had been obtained experimentally and then to continue the simulation of these data beyond that which could be provided by experiment. This is for materials in a stress-relaxed state. A problem for precise loading of laboratory fracture specimens to achieve fast cracks is that there can be time for the specimens to exhibit some yielding or crazing prior to crack initiation. The experimental fracture data, therefore, was obtained for loading conditions below the yield or craze threshold of each material. Modelling was then used to extend the experimental relationship between crack velocity and stress up to the limiting crack velocity condition, for each material. This is so that the needed comparisons could be made between the different materials over the full crack velocity range. The faster the crack then the smaller the zone about the tip of the crack that has time to provide the crack tip with strain energy. Hence, yielding or crazing starting outside this zone has limited effect and that occurring inside this zone is very much part of the fracture process. As the crack approaches the limiting velocity condition the more confined are crack tip fracture processes. Also, there is less time for material ahead of the crack tip to be aware of its presence and able to respond to crack tip stresses. However, there are loading conditions when continuous fast crack propagation can be maintained and an example is given in reference [11]. When researching toughening agents it is often their effect over the full crack velocity range that is needed.

2. Modelling studies

The model consisted of columns and arrays of mass-spring elements with the masses also being linked by diagonal springs as illustrated in Fig. 1. This is with each spring in parallel with a damping element. This construction includes provision for Poisson's contraction and expansion effects. The uniform structure provides for good wave propagation characteristics. Each mass

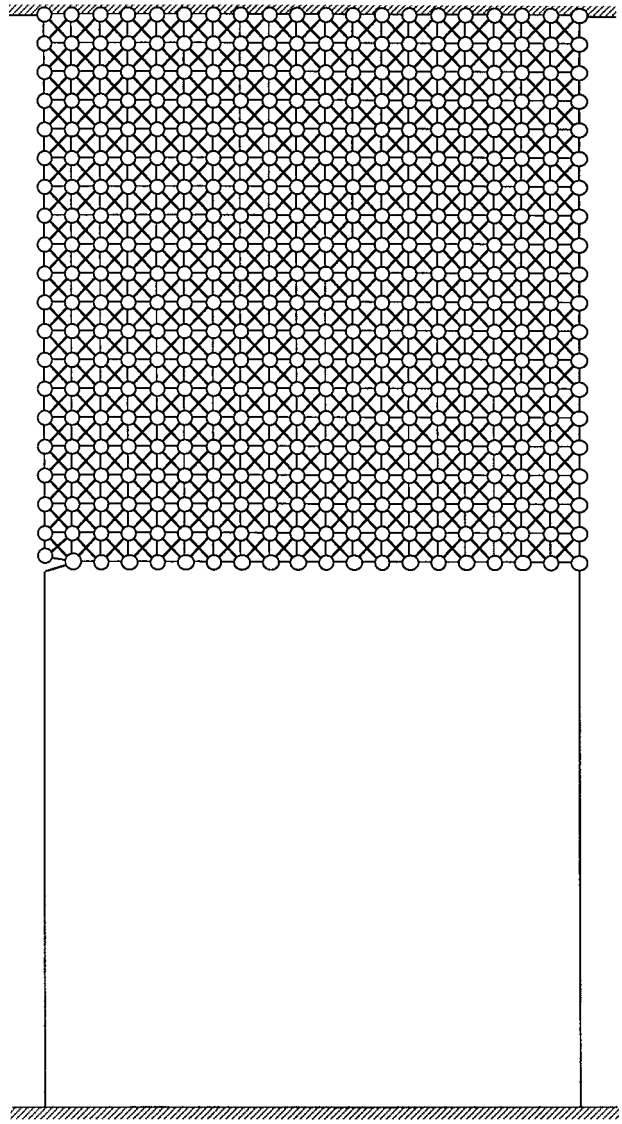

Figure 1 Distributed mass-spring network, for one half of a fracture specimen, showing initial position of masses, horizontal, vertical and cross-diagonal spring elements with mass positions – $\underset{\sim}{r}_{ij}$ $\{i = 1$ to 20 *(top to bottom)* and $j = 1$ to 20 *(left to right)*$\}$. The mass displacements for $i = 1$ were held fixed to simulate the fixed grip condition of the frozen tongue specimen and the mass displacements for $i = 20$ were fixed initially in the vertical direction (*as required by symmetry*) and then released as bonds were broken along the crack path.

is free to move in the two-dimensional plane of the model. Compared with finite element (FE) and other powerful models [12–15] hosted on large computers, the PC distributed mass-spring model has its limitations but it was well able to provide, for example, the following:

- The simulation of stress intensity and its distribution about a propagating crack tip for velocities up to the shear wave velocity.
- The simulation of the toughness of different materials including the effect of micro-cracks and other failure processes occurring at and about the crack tip.
- The simulation of the generation of dynamic strain energy from the stored static strain energy in the specimen and the transfer of this dynamic strain energy to the crack tip for materials of different toughness.

- The simulation of a crack growing from a small fault and reaching steady state crack propagation conditions that relate to the stored static strain energy in the specimen.

A limitation of distributed mass-spring modelling is that it is not so versatile as FE modelling which can accommodate better, for example, visco-elasticity and three-dimensional effects. However, for these fracture studies, the distributed mass-spring model as used here, is not affected by these shortcomings. This is because the experimental material specimens are required to be in nearly fully stress relaxed state before crack initiation and the time constant of any subsequent relaxation is large compared with the fast fracture processes about the crack tip. With regards to three-dimensional effects, the experimental material specimens are side-grooved to achieve close to plane strain fracture conditions. Hence, the two-dimensional distributed mass-spring model used is well able to simulate these plane strain fracture processes.

When the distributed mass-spring model is tensioned, normal to the crack path, strain energy is initially stored in the vertical and horizontal springs (T) as well as the cross-diagonal springs (S) with the vertical and cross-diagonal springs being in tension and the horizontal springs being in compression (see Fig. 2). When the crack is propagating and the masses along the designated crack path are sequentially released, there is a dynamic transfer of strain energy through the mass-spring network to the crack tip. PC machines are well able to do step-by-step integration to represent this dynamic strain energy transfer process. This is the process resulting in a build-up of strain energy at and ahead of the crack tip. The rate and extent of the redistribution and build-up of dynamic strain energy at the crack tip is thus determined by the response characteristics of the distributed mass-spring network. It follows that the faster the crack bonds are broken, the less time there is for the network to transfer strain energy to the advancing crack tip. The Poisson's ratio of the material to be represented determines the relative stiffness of the T and S springs. Similarly, the PC model's mass, distributed viscous damping and energy-absorbing elements at the crack tip are related to the material to be simulated. Equations of motion for each mass in the modelling network provide a basis for a step-by-step program to compute the motion of the sprung masses as the crack moves along a designated path. For the model that is shown in Fig. 1, the equation of motion for each mass is as follows:

$$
\begin{aligned}
&m\frac{\mathrm{d}^2\underline{r}_{ij}}{\mathrm{d}t^2}\\
&= k_T(|\underline{r}_{i-1j}-\underline{r}_{ij}|-L_0)\frac{(\underline{r}_{i-1j}-\underline{r}_{ij})}{|\underline{r}_{i-1j}-\underline{r}_{ij}|}\\
&\quad + k_T(|\underline{r}_{i+1j}-\underline{r}_{ij}|-L_0)\frac{(\underline{r}_{i+1j}-\underline{r}_{ij})}{|\underline{r}_{i+1j}-\underline{r}_{ij}|}\\
&\quad + k_T(|\underline{r}_{ij-1}-\underline{r}_{ij}|-L_0)\frac{(\underline{r}_{ij-1}-\underline{r}_{ij})}{|\underline{r}_{ij-1}-\underline{r}_{ij}|}\\
&\quad + k_T(|\underline{r}_{ij+1}-\underline{r}_{ij}|-L_0)\frac{(\underline{r}_{ij+1}-\underline{r}_{ij})}{|\underline{r}_{ij+1}-\underline{r}_{ij}|}\\
&\quad + k_S(|\underline{r}_{i-1j-1}-\underline{r}_{ij}|-\sqrt{2}L_0)\frac{(\underline{r}_{i-1j-1}-\underline{r}_{ij})}{|\underline{r}_{i-1j-1}-\underline{r}_{ij}|}\\
&\quad + k_S(|\underline{r}_{i-1j+1}-\underline{r}_{ij}|-\sqrt{2}L_0)\frac{(\underline{r}_{i-1j+1}-\underline{r}_{ij})}{|\underline{r}_{i-1j+1}-\underline{r}_{ij}|}\\
&\quad + k_S(|\underline{r}_{i+1j-1}-\underline{r}_{ij}|-\sqrt{2}L_0)\frac{(\underline{r}_{i+1j-1}-\underline{r}_{ij})}{|\underline{r}_{i+1j-1}-\underline{r}_{ij}|}\\
&\quad + k_S(|\underline{r}_{i+1j+1}-\underline{r}_{ij}|-\sqrt{2}L_0)\frac{(\underline{r}_{i+1j+1}-\underline{r}_{ij})}{|\underline{r}_{i+1j+1}-\underline{r}_{ij}|}\\
&\quad + \eta_T\left(\frac{\mathrm{d}|\underline{r}_{i-1j}-\underline{r}_{ij}|}{\mathrm{d}t}\right)\frac{(\underline{r}_{i-1j}-\underline{r}_{ij})}{|\underline{r}_{i-1j}-\underline{r}_{ij}|}\\
&\quad + \eta_T\left(\frac{\mathrm{d}|\underline{r}_{i+1j}-\underline{r}_{ij}}{\mathrm{d}t}\right)\frac{(\underline{r}_{i+1j}-\underline{r}_{ij})}{|\underline{r}_{i+1j}-\underline{r}_{ij}|}\\
&\quad + \eta_T\left(\frac{\mathrm{d}|\underline{r}_{ij-1}-\underline{r}_{ij}|}{\mathrm{d}t}\right)\frac{(\underline{r}_{ij-1}-\underline{r}_{ij})}{|\underline{r}_{ij-1}-\underline{r}_{ij}|}\\
&\quad + \eta_T\left(\frac{\mathrm{d}|\underline{r}_{ij+1}-\underline{r}_{ij}}{\mathrm{d}t}\right)\frac{(\underline{r}_{ij+1}-\underline{r}_{ij})}{|\underline{r}_{ij+1}-\underline{r}_{ij}|}\\
&\quad + \eta_S\left(\frac{\mathrm{d}|\underline{r}_{i-1j-1}-\underline{r}_{ij}|}{\mathrm{d}t}\right)\frac{(\underline{r}_{i-1j-1}-\underline{r}_{ij})}{|\underline{r}_{i-1j-1}-\underline{r}_{ij}|}\\
&\quad + \eta_S\left(\frac{\mathrm{d}|\underline{r}_{i-1j+1}-\underline{r}_{ij}}{\mathrm{d}t}\right)\frac{(\underline{r}_{i-1j+1}-\underline{r}_{ij})}{|\underline{r}_{i-1j+1}-\underline{r}_{ij}|}\\
&\quad + \eta_S\left(\frac{\mathrm{d}|\underline{r}_{i+1j-1}-\underline{r}_{ij}|}{\mathrm{d}t}\right)\frac{(\underline{r}_{i+1j-1}-\underline{r}_{ij})}{|\underline{r}_{i+1j-1}-\underline{r}_{ij}|}\\
&\quad + \eta_S\left(\frac{\mathrm{d}|\underline{r}_{i+1j+1}-\underline{r}_{ij}}{\mathrm{d}t}\right)\frac{(\underline{r}_{i+1j+1}-\underline{r}_{ij})}{|\underline{r}_{i+1j+1}-\underline{r}_{ij}|} \qquad (1)
\end{aligned}
$$

where the position vector of each mass (m) is $\underline{r}_{ij}$ and L_0 is the initial spacing of the masses in the unstressed spring network. The stiffness of the horizontal and vertical springs (T) and cross-diagonal springs (S) are k_T and k_S respectively with damping η_T for the horizontal and vertical (T) springs and damping η_S for the cross-diagonal (S) springs. Each element in the model would need to relate to the size and properties of a corresponding element in the material being simulated and the

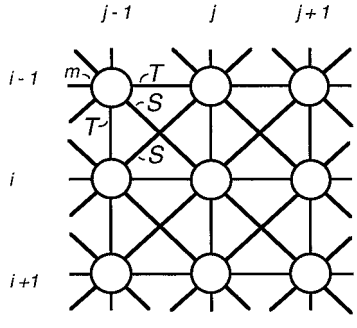

Figure 2 Detail of mass-spring network showing the vertical and horizontal springs (T) as well as the cross-diagonal springs (S) with mass positions – $\underline{r}_{ij}$ {$i = 1$ to 20 and $j = 1$ to 20}.

following relationships particularly need to be taken into account:

$$m = \rho B L_0^2, \quad \eta_T = 2\xi\sqrt{k_T m}, \quad \eta_S = 2\xi\sqrt{k_S m}$$
$$\frac{\left[(k_T + k_S)^2 - k_S^2\right]}{(k_T + k_S)} = EB, \quad \frac{k_S}{(k_T + k_S)} = \nu \quad (2)$$
$$C_S = L_0\sqrt{\frac{ks}{m}}, \quad C_0 = L_0\sqrt{\frac{(k_T + k_S)}{m}}$$

where ρ is density, E is the Young's modulus of the bulk material, ν is Poisson's ratio, C_S is the shear wave velocity, C_0 is the longitudinal wave velocity, B is the specimen thickness and ξ is the non-dimensional damping ratio for the T and S springs. The ratio of k_S/k_T relates to the Poisson's ratio of the material being studied ($k_S/k_T = \nu/(1-\nu)$). When making specific comparisons between different materials but identically shaped specimens then the equations can be simplified by normalisation. A modelling point is that care is needed in selecting a suitably small time-step to keep the build-up of computational error to an acceptable level. This is particularly important when the transient behaviour of the structure is complex.

The crack tip conditions can be modelled in several ways but the version used here was the same as that often employed in FE and other studies [13, 14]. One feature is to provide an energy sink and a smooth opening of the crack tip by applying a decaying hold-back force to each crack path mass as its bond is broken. At any time, the hold-back force, F_{hold}, is applied to one released crack path mass and is allowed to decay linearly or to some other law as given by:

$$F_{\text{hold}} = -F_0\left[1 - \frac{d}{L}\right]^s \quad (3)$$

where F_0 is the force on the crack tip mass at its moment of release, L is the spacing of the masses along the crack path, d is the increment of crack growth from the last release of a crack tip mass and s is unity for a linear decay. The other crack tip feature of the model is to change dynamically the effective modulus (E_c) of the elements immediately about the advancing crack tip to represent, for example, local yielding or crazing of the material around the crack tip. The reduction in crack tip effective modulus (E_c) was achieved by reducing the stiffness of the model's springs (k_T and k_S) immediately and only about the tip of the propagating crack. This includes the effects of yielding, crazing, micro-cracking, drawing of fibrils, the generation of a hot spot and other energy absorbing processes in the zone about the crack tip. These features simulate the toughness of the material or the energy absorbed at the crack tip and also the change in material properties in the crack tip zone as produced or enhanced by toughening agents.

The effects of using different sizes of mesh were explored before deciding on the arrangement of 20 by 20 mass-spring elements. This size of mesh provided good simulation results that were close to the experimental fracture data observed. Further increasing the number of mass-spring elements, to represent the same specimen size, did not offer improvements. It is to be noted that a sufficient number of mesh elements are needed to obtain a good simulation of the distortion of the material about the crack tip. However, not to be overlooked, is that the faster the crack, then, the smaller the zone about the crack tip that is able to provide strain energy to the advancing crack tip.

The dynamic strain energy release rate, G_{dyn}, is given by:

$$G_{\text{dyn}} = \frac{1}{B}\left[\frac{\mathrm{d}U_e}{\mathrm{d}a} - \frac{\mathrm{d}U_s}{\mathrm{d}a} - \frac{\mathrm{d}U_k}{\mathrm{d}a} - \frac{\mathrm{d}U_d}{\mathrm{d}a}\right] \quad (4)$$

where B is thickness, a is crack length, U_e is external work done, U_s is the total stored strain energy, U_k is the total kinetic energy and U_d is the dissipated energy in the distributed viscous damping elements. For the fixed grip geometry shown, there is no external work done (U_e) during the crack growth. The total strain energy (U_s), total kinetic energy (U_k) and dissipated energy in the distributed viscous damping elements (U_d) are given by:

$$\begin{aligned} U_s = &\sum_{i=1}^{19}\sum_{j=1}^{19}\frac{1}{2}k_T(|\underline{r}_{i+1j} - \underline{r}_{ij}| - L_0)^2 \\ &+ \sum_{i=1}^{19}\sum_{j=1}^{19}\frac{1}{2}k_T(|\underline{r}_{ij+1} - \underline{r}_{ij}| - L_0)^2 \\ &+ \sum_{i=1}^{19}\sum_{j=1}^{19}\frac{1}{2}k_S(|\underline{r}_{i+1j+1} - \underline{r}_{ij}| - \sqrt{2}L_0)^2 \\ &+ \sum_{i=1}^{19}\sum_{j=1}^{19}\frac{1}{2}k_S(|\underline{r}_{ij+1} - \underline{r}_{i+1j}| - \sqrt{2}L_0)^2 \end{aligned} \quad (5)$$

$$U_k = \sum_{i=1}^{20}\sum_{j=1}^{20}\frac{1}{2}m\left|\frac{\mathrm{d}\underline{r}_{ij}}{\mathrm{d}t}\right|^2 \quad (6)$$

$$\begin{aligned} U_d = &\sum_{i=1}^{19}\sum_{j=1}^{19}\int_{t'=0}^{t}\eta_T\left(\frac{\mathrm{d}|\underline{r}_{i+1j} - \underline{r}_{ij}|}{\mathrm{d}t'}\right)^2\mathrm{d}t' \\ &+ \sum_{i=1}^{19}\sum_{j=1}^{19}\int_{t'=0}^{t}\eta_T\left(\frac{\mathrm{d}|\underline{r}_{ij+1} - \underline{r}_{ij}|}{\mathrm{d}t'}\right)^2\mathrm{d}t' \\ &+ \sum_{i=1}^{19}\sum_{j=1}^{19}\int_{t'=0}^{t}\eta_S\left(\frac{\mathrm{d}|\underline{r}_{i+1j+1} - \underline{r}_{ij}|}{\mathrm{d}t'}\right)^2\mathrm{d}t' \\ &+ \sum_{i=1}^{19}\sum_{j=1}^{19}\int_{t'=0}^{t}\eta_S\left(\frac{\mathrm{d}|\underline{r}_{ij+1} - \underline{r}_{i+1j}|}{\mathrm{d}t'}\right)^2\mathrm{d}t' \end{aligned} \quad (7)$$

so G_{dyn} can be obtained from the distributed mass-spring model using the energy balance in Equation 4. To confirm this analysis, G_{dyn} can also be determined as the work done against the holdback force, U_{hold}, which resists the opening of the crack as each crack path mass is released:

$$U_{\text{hold}} = \sum_{j=1}^{z} \int_{t'=0}^{t} F_{\text{hold}}\, \underline{n} \cdot \left(\frac{\mathrm{d}\underline{r}_{20j}}{\mathrm{d}t'} \right)_{\text{hold}} \mathrm{d}t' \qquad (8)$$

$$G_{\text{dyn}} = \frac{1}{B}\left[\frac{\mathrm{d}U_{\text{hold}}}{\mathrm{d}a} \right] \qquad (9)$$

where F_{hold} is the hold-back force defined by Equation 3, $\underline{n}$ is a unit vector in the plane of the specimen normal to the direction of crack propagation and z is the number of crack path masses released. For this study, the generation mode was employed to obtain dynamic energy release rates (G_{dyn}) for different crack velocities for polymeric materials with and without toughening agents.

3. Experimental studies

In this research, rectangular specimens of ABS, SAN, HIPS and PS were provided with a small tongue extension, at the beginning of the crack path, so that the frozen tongue technique [9, 10] could be used to fracture the material. The specimens were side-grooved to minimise side-lip tearing so as to achieve, in the centre of the fracture surfaces, as near to plane strain conditions as possible. For each material, crack velocity versus applied stress curves were obtained under steady state fracture conditions. This is from the threshold static stress for crack propagation up to the limiting crack velocity condition or as high a crack velocity as was possible.

The frozen tongue technique takes advantage of the good thermal insulation properties of polymers, which permits a small tongue of material, at the beginning of the crack path, to be freeze-cooled with liquid nitrogen so that a crack can easily be initiated in the tongue with a low force device. The freezing of the tongue and the application of the crack initiation force were confined to the half of the tongue furthest from the main section of the specimen. It was verified that this crack initiation procedure only caused a very small change in the stress and temperature for the first 5% of the crack path in the main section of the specimen [9]. It was possible, from a series of experiments, each with different loading of the main section, to determine the threshold static stress, which will just maintain crack propagation in the material. Also, how crack velocity varied with increasing stress up to the limiting condition or the highest crack velocity possible. Fig. 3 illustrates the frozen tongue technique including the three-point bend method for starting a sharp crack in the frozen tongue. The dimensions of the stressed main section, for the frozen tongue specimens, were width (W) = 90 mm, height (H) = 180 mm and thickness (B) = 6 mm. The dimensions of the tongue section of the specimen were 40 mm by 40 mm. Side grooves of depth 1 mm were used on all the specimens to provide for near to plane-strain fracture conditions. Prior to crack initiation, the main section of the frozen tongue specimen was loaded at a constant strain rate of 5 mm min^{-1} using an Instron tensile loading machine. At the required load, the machine cross-head was stopped and the specimen allowed to stress relax. After cooling of the tongue,

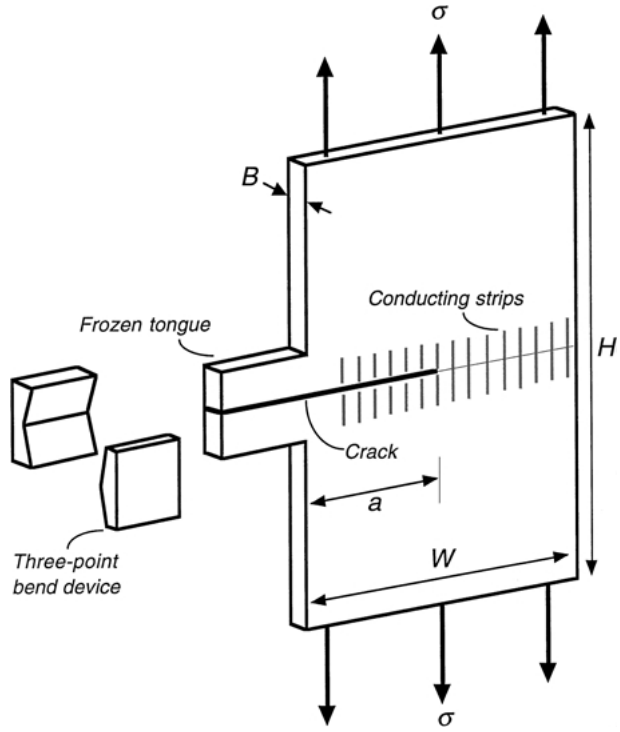

Figure 3 Frozen tongue specimen geometry. The width (W) of the stressed main section of the specimen is 90 mm, the height (H) 180 mm and the thickness (B) 6 mm. The tongue is 40 mm by 40 mm (three-point bend device for crack initiation shown). The instrumentation consists of conducting strips to record crack velocity.

a crack was then initiated using the low-force, static three-point bend loading device. For each static stress level, in the main section, crack velocity was measured using a combination of high-speed photography and on-specimen instrumentation. The on-specimen instrumentation consisted of a series of conducting strips monitors, which were located along the crack path as shown in Fig. 3. It was found important to achieve a sharp and clean breaking of the conducting strips across the crack path, which had to be strong enough not to be damaged when handling and mounting in the Instron testing machine. Two separate sets of conducting strip monitoring were formed with one on each side of the specimen to obtain confirmatory outputs. The breaking of the conducting strips produced outputs that were monitored by a Digital Storage Scope (Gould—DataSYS 740). This was equipped with facilities for transfer of the crack velocity data to a personal computer (PC). The crack velocity measurement was confirmed using high-speed photography (image converter IMACON 468 camera) with backlighting so that the crack appeared as a bright streak of light passing through the specimen. Both measurement techniques showed that the crack upon leaving the tongue travelled at near to constant velocity across the full width of the specimen.

4. Results

The need was to be able to operate the model to study fracture processes at different crack velocities in ABS, SAN, HIPS and PS. This is for constant crack velocities from the threshold static stress to just maintain crack propagation up to the limiting crack velocity condition

related to the shear wave velocity (C_S) of the material. For all these crack propagation simulations, the aspect ratio, of crack path length (W) relative to specimen height (H), was the same as that used for the frozen tongue experiments.

Fig. 4 shows, for crack velocities ($\mathrm{d}a/\mathrm{d}t$) of $0.4C_S$ and $0.6C_S$, the expenditure of the total strain energy (U_s) of the mass-spring network to work done at the crack tip (U_{hold}) and that remaining as kinetic energy (U_k) in the masses as the crack length increases. The values of U_s, U_k and U_{hold} were determined from Equations 5, 6 and 8 respectively. In each case, these quantities are normalised with respect to the initial strain energy (U_0) given to the model by the external applied stress. At low crack velocities (less than $0.4C_S$), little kinetic energy is given to the masses. However, the kinetic energy imparted to the masses increases with crack velocity and this is with kinetic energy fluctuations due to dynamic effects. These kinetic energy (U_k) fluctuations are also revealed in the total strain energy (U_s) curve.

Fig. 5 shows for a crack velocity of $0.6C_S$ the movement of the masses in the mass-spring network that relate to the opening of the crack when the crack length, a, is $0.25W$, $0.5W$ and $0.75W$. This shows the region about the crack tip that can provide strain energy to the propagating tip. It is to be noted that fracture data used in analysis was only when there was no distortion evident at the vertical sides of the specimen and the crack was long enough for the full crack profile to have been achieved ($a = 0.5W$).

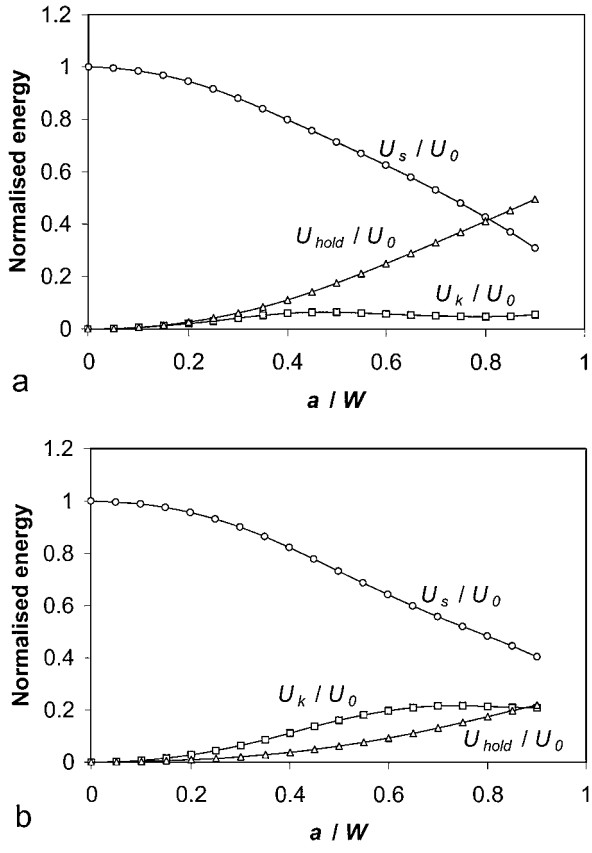

Figure 4 Normalised plots of total strain energy (U_s/U_0), total kinetic energy (U_k/U_0) and work done against hold-back force (U_{hold}/U_0) where U_0 is the initial strain energy versus normalised crack length (a/W) from the distributed mass-spring model ($\nu = 0.36$ and $E_c/E = 1$) for: (a) $\mathrm{d}a/\mathrm{d}t = 0.4C_S$, (b) $\mathrm{d}a/\mathrm{d}t = 0.6C_S$.

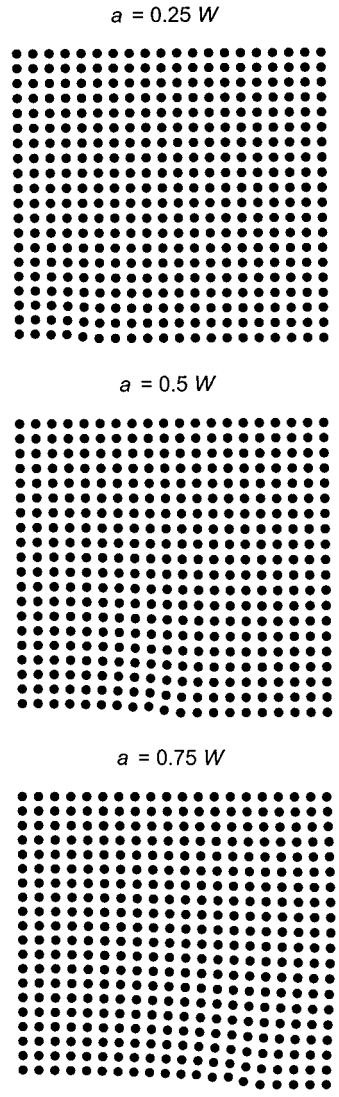

Figure 5 Distributed mass-spring simulation model ($\nu = 0.36$ and $E_c/E = 1$) showing the position of the masses when $a = 0.25W, 0.5W$ and $0.75W$ for $\mathrm{d}a/\mathrm{d}t = 0.6C_S$ (mass displacements magnified so that the movement can be more clearly seen).

Modelling simulations were then performed to study separately the effect of changing the toughness and the Poisson's ratio (ν) of the material. This is as appropriate for studying ABS, SAN, HIPS and PS. Fig. 6 shows curves for the normalised dynamic energy release rate ($G_{\text{dyn}}/G_{\text{static}}$) plotted versus normalised crack velocity ($\mathrm{d}a/\mathrm{d}t/C_S$) obtained from the distributed mass-spring model for different crack tip toughness conditions. Fig. 6a shows, for a material with Poisson's ratio (ν) of 0.39, the change in $G_{\text{dyn}}/G_{\text{static}}$ as the crack tip velocity ($\mathrm{d}a/\mathrm{d}t$) increases towards the shear wave velocity (C_S) for different crack tip toughness. The uppermost of the curves for $G_{\text{dyn}}/G_{\text{static}}$ versus $\mathrm{d}a/\mathrm{d}t/C_S$ relates to the case when there is no reduction of the material's modulus occurring about the crack tip. This represents $E_c/E = 1$ where E_c is the Young's modulus of the material immediately about the crack tip and E is the Young's modulus of the bulk material. The lower three curves of $G_{\text{dyn}}/G_{\text{static}}$ versus $\mathrm{d}a/\mathrm{d}t/C_S$ are for reductions in modulus of the elements immediately about the tip of the crack such that $E_c/E = 0.5$, 0.25 and 0.125 respectively. For these three lower curves, the reduction in crack tip modulus (E_c) was achieved

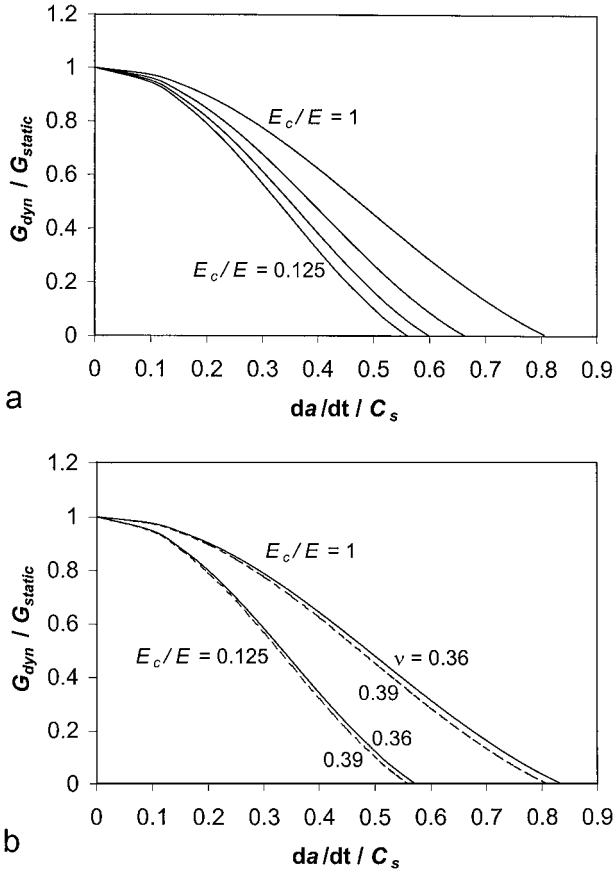

Figure 6 Normalised dynamic energy release rate ($G_{\text{dyn}}/G_{\text{static}}$) versus normalised crack velocity ($\mathrm{d}a/\mathrm{d}t/C_S$) from the distributed mass-spring model for: (a) $\nu = 0.39$ and $E_c/E = 1$, $E_c/E = 0.5$, $E_c/E = 0.25$ and $E_c/E = 0.125$. (b) $\nu = 0.36$ (solid curve) compared with $\nu = 0.39$ (dashed curve) when $E_c/E = 1$ and $E_c/E = 0.125$.

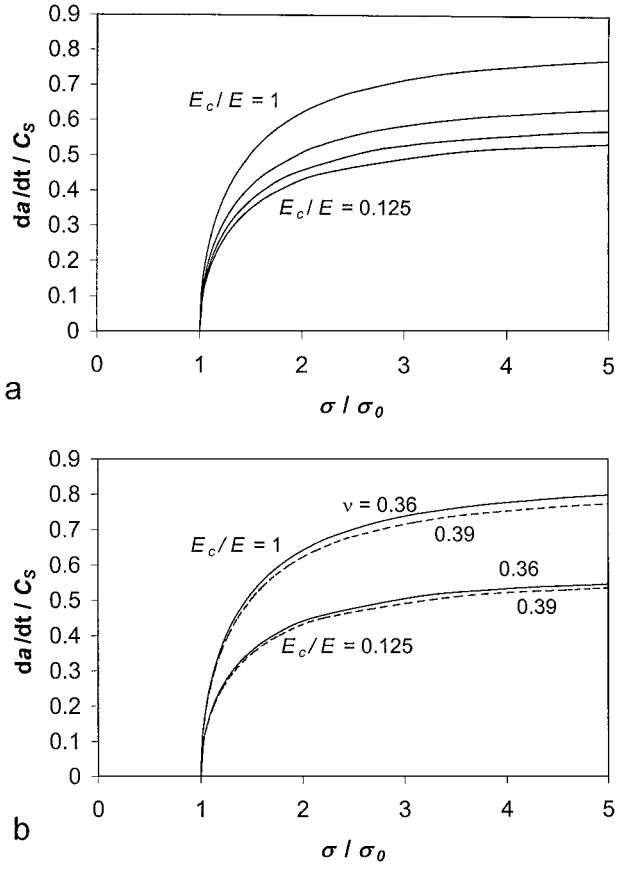

Figure 7 Normalised crack velocity ($\mathrm{d}a/\mathrm{d}t/C_S$) versus normalised static stress (σ/σ_0) from the distributed mass-spring model for: (a) $\nu = 0.39$ when $E_c/E = 1$, $E_c/E = 0.5$, $E_c/E = 0.25$ and $E_c/E = 0.125$. (b) $\nu = 0.36$ (solid curve) compared with $\nu = 0.39$ (dashed curve) when $E_c/E = 1$ and $E_c/E = 0.125$.

by reducing the stiffness of the model's springs (k_T and k_S), immediately and only about the tip of the propagating crack. This is to simulate yielding, crazing and other energy absorbing processes in the material about the tip of the propagating crack. The simulation data in Fig. 6a shows that this results in a reduction of the limiting crack velocity (C_L) possible. Fig. 6b shows the different effect of varying the Poisson's ratio (ν) of the bulk material from 0.39 to 0.36 on the $G_{\text{dyn}}/G_{\text{static}}$ versus $\mathrm{d}a/\mathrm{d}t/C_S$ curves. This is for the two conditions of $E_c/E = 1$ and $E_c/E = 0.125$. It is noted that the limiting crack velocity (C_L) is altered by a change in the Poisson's ratio (ν). The Poisson's ratio (ν), for the polymers in this study, only ranges from 0.36 (SAN and PS) to 0.39 (ABS and HIPS). Hence there is only a small change in the limiting crack velocity relating to Poisson's ratios of these materials. In the model, the Poisson's ratio relates to the stiffness of the vertical and horizontal (T) springs and cross-diagonal (S) springs (k_T and k_S respectively).

The simulation data of Fig. 6 for normalised dynamic energy release rate ($G_{\text{dyn}}/G_{\text{static}}$) versus normalised crack velocity ($\mathrm{d}a/\mathrm{d}t/C_S$) can be converted into plots of normalised crack velocity ($\mathrm{d}a/\mathrm{d}t/C_S$) versus normalised stress (σ/σ_0) as shown in Fig. 7. This is achieved by using the following relationship:

$$\frac{G_{\text{dyn}}}{G_{\text{static}}} = \left(\frac{\sigma_0}{\sigma}\right)^2 \tag{10}$$

where σ is the static stress on the specimen and σ_0 is the threshold value of the static stress to just sustain crack propagation in the material. This is based on the Griffith relationship that G_{static} varies as $\sigma^2 a/E$ where σ is the static stress on the specimen, a is the crack length and E is the Young's modulus of the bulk material. Also, G_{dyn} varies as $\sigma_0^2 a/E$ where σ_0 is the threshold static stress to just sustain crack propagation since G_{dyn} is equal to the fracture resistance of the material.

Fig. 7a shows $\mathrm{d}a/\mathrm{d}t/C_S$ versus σ/σ_0 from the distributed mass-spring model for $\nu = 0.39$ when $E_c/E = 1$, 0.5, 0.25 and 0.125. It is to be noted that the reduction in modulus (E_c) at crack tip which simulates yielding, crazing and other energy absorbing processes in the material about the crack tip leads to a reduction in limiting crack velocity. Fig. 7b shows the effect of varying the Poisson's ratio (ν) of the bulk material from 0.39 to 0.36 on the normalised crack velocity ($\mathrm{d}a/\mathrm{d}t/C_S$) versus normalised stress (σ/σ_0) curves for the two conditions of $E_c/E = 1$ and $E_c/E = 0.125$. Changes in the Poisson's ratio (ν) of the bulk material produce small changes in the $\mathrm{d}a/\mathrm{d}t/C_S$ versus σ/σ_0 curve. The dominant effect is produced by the dynamic reduction of the modulus (E_c) of the material at the crack tip.

Fig. 8 shows the crack velocity ($\mathrm{d}a/\mathrm{d}t$) versus static stress (σ) data for the frozen tongue fracture of materials researched in this study. For specimen stresses less

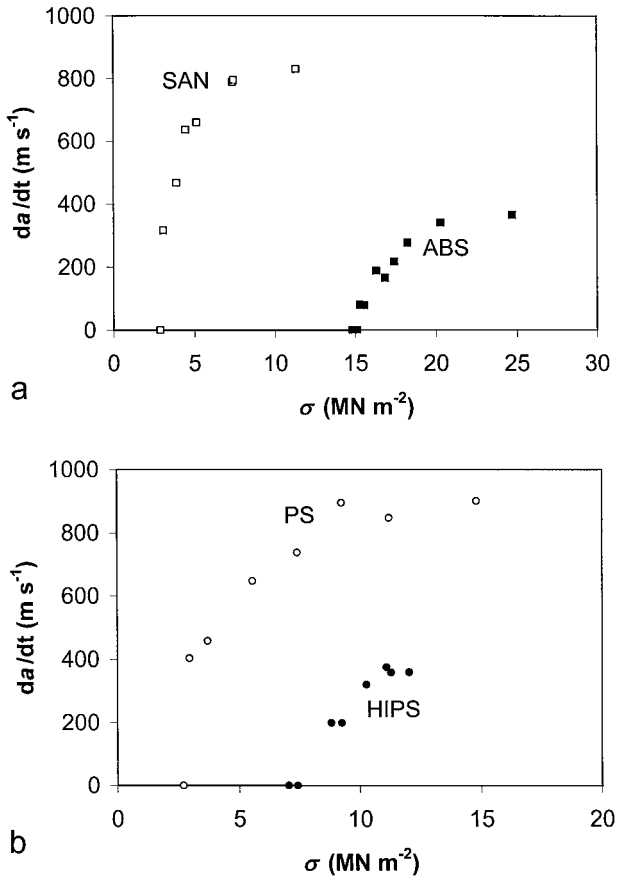

Figure 8 Crack velocity, da/dt, versus static stress, σ, at crack initiation for frozen tongue experiments showing the threshold static stress σ_0 for crack propagation (given in Table I) for: (a) SAN(□) and ABS(■)—the yield point for ABS is shown, (b) PS(○) and HIPS(●)—the yield point for HIPS is shown.

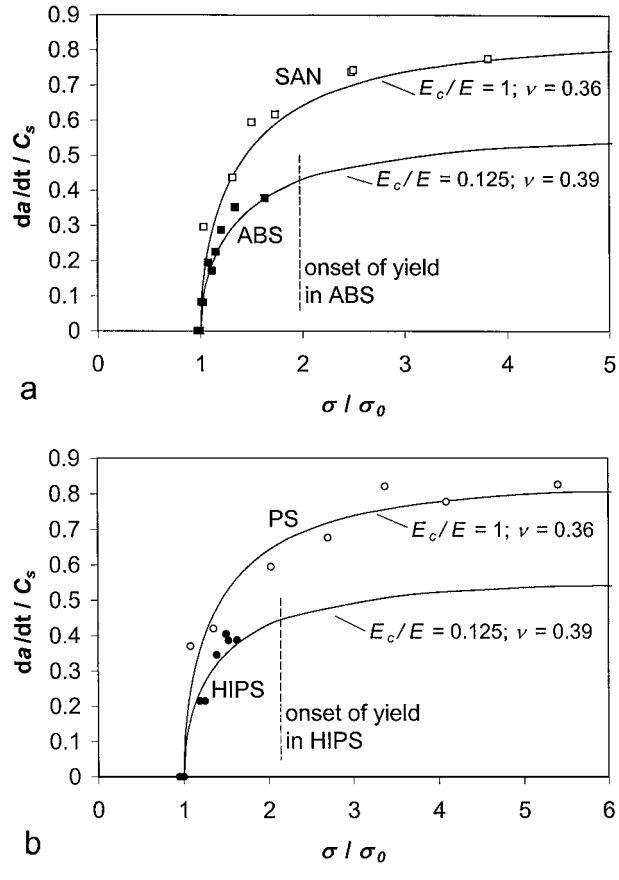

Figure 9 Normalised dynamic energy release rate (G_{dyn}/G_{static}) versus normalised crack velocity ($da/dt/C_S$) distributed mass-spring model curves together with frozen tongue data for: (a) SAN(□) and ABS(■), (b) PS(○) and HIPS(●).

than σ_0, sustained crack propagation did not occur and the crack arrested in the specimen. These are evident as data-points on the horizontal axis of Fig. 8. For specimens stressed above σ_0, sustained crack propagation at a constant velocity was observed as measured with conducting strips and high-speed photography. These measurements define the threshold stress, σ_0, for crack propagation in ABS and SAN (Fig. 8a) and HIPS and PS (Fig. 8b) as recorded in Table I. The Young's modulus, E, and Poisson's ratio, ν, for ABS, SAN, HIPS and PS were determined using longitudinal and transverse wave velocity measurements for an excitation frequency of 2 MHz and the density, ρ, and the yield (or craze) stress, σ_y, for each material was from manufacturer's verified data. From these data, the shear wave velocity ($C_S = (E/2(1+\nu)\rho)^{1/2}$) was determined and the results are also summarised in Table I.

Fig. 9 shows normalised crack velocity ($da/dt/C_S$) versus normalised static stress (σ/σ_0) from the distributed mass-spring model curves together with normalised frozen tongue data for ABS(■) and SAN(□) (Fig. 9a) and HIPS(●) and PS(○) (Fig. 9b). The data for SAN and PS ($\nu = 0.36$) is appropriately near the model's curve for $\nu = 0.36$ and $E_c/E = 1$ (upper curve) and the data for ABS and HIPS ($\nu = 0.39$) is close to the model's curve for $\nu = 0.39$ and $E_c/E = 0.125$ (lower curve). On the ABS and HIPS curves, vertical dashed lines (marked in Fig. 9a and b) indicate the onset of noticeable yielding of the bulk material. It is to be noted, however, that there is some partial drawing and yielding of these materials prior to the full yielding of the bulk material starting. The bulk yielding of the material limits the stress range over which experimental data for sustained crack propagation can be obtained in ABS and HIPS and means it is difficult to achieve experimental crack velocities up to the limiting crack velocity for these toughened materials.

Fig. 10 shows normalised dynamic energy release rate (G_{dyn}/G_{static}) versus normalised crack velocity

TABLE I Data for threshold stress (σ_0) *from frozen tongue experiments*, Young's modulus of the bulk material (E) and Poisson's ratio (ν) *from wave velocity measurements*, density (ρ) and yield (or craze) stress (σ_y) *from manufacturer's verified data* and shear wave velocity ($C_S = E/2(1+\nu)\rho)^{1/2}$)

Material	σ_0 (MN m^{-2})	σ_y (MN m^{-2})	E (GN m^{-2})	ν	ρ (kg m^{-3})	C_S (m s^{-1})
ABS	15.2	45	2.7	0.39	1040	970
SAN	3.0	70	3.3	0.36	1060	1070
HIPS	7.4	35	2.5	0.39	1040	930
PS	2.7	50	3.4	0.36	1050	1090

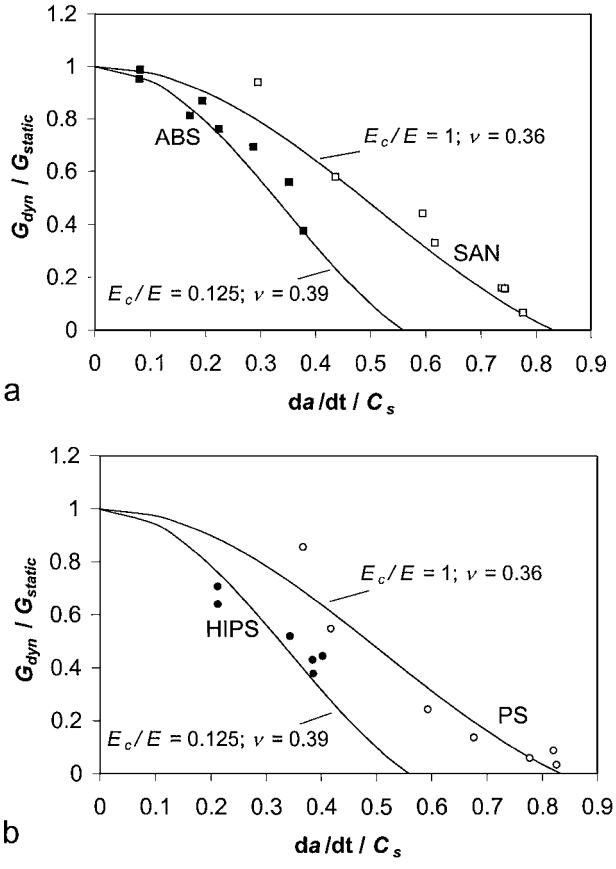

Figure 10 Normalised crack velocity ($da/dt/C_S$) versus normalised static stress (σ/σ_0) from the distributed mass-spring model together with frozen tongue data for: (a) SAN(□) and ABS(■)—onset of yield for ABS is shown, (b) PS(○) and HIPS(●)—onset of yield for HIPS is shown.

($da/dt/C_S$) distributed mass-spring model curves together with frozen tongue data (using Equation 10) for ABS(■) and SAN(□) (Fig. 10a) and HIPS(●) and PS(○) (Fig. 10b). As shown in Fig. 9, the data for SAN and PS ($\nu = 0.36$) is appropriately near the model's curve for $\nu = 0.36$ and $E_c/E = 1$ to give a limiting crack velocity (C_L) of $\sim 0.8C_S$. Also, the data for ABS and HIPS ($\nu = 0.39$) is close to the model's curve for $\nu = 0.39$ and $E_c/E = 0.125$ to give a limiting crack velocity (C_L) of $\sim 0.55C_S$.

This marked reduction of the limiting crack velocity (C_L) from $\sim 0.8C_S$ for SAN and PS to $\sim 0.55C_S$ for HIPS and ABS relates to the toughening effect of the rubber particles. It is to be noted (in Table I) that the bulk values of Young's modulus of ABS and HIPS (2.7 GN m^{-2} and 2.5 GN m^{-2} respectively) are only a little less than the bulk values of Young's modulus of SAN and PS (3.3 GN m^{-2} and 3.4 GN m^{-2} respectively). As a result, the shear wave velocities (C_S) are not greatly different. The main toughness effect of the ABS rubber particles is within the crack tip zone, which relates to the reduction in crack tip modulus used in the distributed mass-spring model to represent ABS and other tough materials. It is evident from this study that C_L for ABS and HIPS relates to the local crack tip modulus (E_c), which is less than the bulk modulus of the material.

5. Discussion

A great deal of research has and is being devoted to producing polymeric materials with strength, stiffness, toughness, density and other required properties to suit different applications. Most material properties are at least partially interrelated and therefore achieving the best overall material formulation can require many experimental and modelling studies. Adding, for example, toughening agents to otherwise brittle polymer can produce a useful and marketable material. This is useful if the toughening agents do not seriously affect other wanted material properties adversely.

In researching toughening methods and possibilities particularly helpful is a combined experimental and computer modelling facility that can be quickly reprogrammed to examine many options. This is to include, for example, being able to study separately the yielding, crazing and other effects of the toughening agents at the crack tip from those occurring elsewhere in the bulk of the material. Often needed is the effect of the toughening agents at the crack tip over the full crack velocity range from the threshold stress to just maintain crack propagation up to the limiting crack velocity conditions. Mostly, this is for the plane strain fracture condition. For tougher materials because of static yielding, crazing or other processes in the bulk of the material, then, obtaining experimental data for the higher crack velocities may not be possible. In these cases, then, to make comparisons of crack tip toughening over the required full crack velocity range, dynamic modelling can usefully be employed to provide a full crack velocity versus stress curve based on the available experimental data for the toughened material. It is to be noted that the material modulus at the crack tip will be different from the bulk modulus because of yielding, crazing, heating and other dynamic softening processes and this is incorporated in the modelling. A consequence of this is that the limiting crack velocity for a toughened material is noticeably more reduced than for the non-toughened material.

A family of complete crack velocity versus stress curves can be generated to represent crack propagation in simulated materials of different toughness but where yielding and other failure processes can only occur at the crack tip. This is when the simulated material, prior to crack propagation, is in a strained but stress relaxed state. Deviations of the experimental data from these simulation curves would occur, for example, with the onset of static yielding or crazing in the experimental material. The combined experimental and computer simulations make it possible to see what would be the changing fracture behaviour of all the different materials evaluated. This is for crack velocities up to the limiting crack velocity condition in the absence of yielding or crazing effects other than those at the crack tip as part of dynamic fracture. It is better to study separately the effects of static yield, crazing and the non-linearity these processes can produce but the results of this study provide some relevant data.

Particularly helpful for these studies, when many comparisons and observations of this kind are needed,

is if the modelling simulation can be hosted on the same PC of modest power as used to capture and process experimental data. Another advantage of the distributed mass-spring modelling is the ease with which it can be changed for different studies and material geometries.

It helps if the needed experimental data can be obtained from material specimens of small size. However, for fracture morphology studies, surfaces are needed that are sufficiently long to show repetitive and other features. The size of specimens used in the frozen tongue technique was chosen to satisfy these different experimental requirements and also to provide for sensors to be attached to the specimens without noticeably affecting the fracture processes.

For ABS and HIPS, the toughening agents are rubber particles. The effects of these rubber particles in these materials are different tending to promote increased yielding in ABS and increased crazing in HIPS. Finding the best size and volume fraction for these toughening agents in host materials is the subject of much research. This is, if possible, to maximise the toughening effects at the tip of a propagating crack without unduly reducing the static load bearing stress of the material before the onset of yielding or crazing occurs. Similar design problems arise with composites and other materials employing one or more different types of material in complex structures to achieve, for example, the required toughness and residual strength after impact damage.

6. Conclusions

The view is that the distributed mass-spring modelling that can be hosted on a PC size of machine, as used to capture experimental data, is a useful and effective way of collectively analysing a variety of fracture research data as it is obtained. This is with the advantage of being able to correlate quickly and frequently modelling and experimental data to guide the course of research. Also, very helpful is the ease of reprogramming the PC model to explore different geometry and other factors affecting the measurement of a material's toughness.

Acknowledgements

The author thanks the Engineering and Physical Sciences Research Council (EPSRC) and Glynwed Plastics (GPS).

References

1. H. SCHARDIN, in "Fracture," edited by B. L. AVERBACH, D. J. K. FELLBECK, G. T. HAHN and D. A. THOMAS (Wiley, New York, 1959) ch. 16.
2. C. S. LEE and M. M. EPSTEIN, *Polym. Eng. Sci.* **22** (1982) 9.
3. C. A. PATON and S. HASHEMI, *J. Mater. Sci.* **27** (1992) 2279.
4. E. C. Y. CHING, W. K. Y. POON, R. K. Y. LI and Y.-W. MAI, *Polym. Eng. Sci.* **40** (2000) 2558.
5. C. B. BUCKNALL and R. R. SMITH, *Polymer* **6** (1965) 437.
6. C. B. BUCKNALL, *Adv. Polymer Sci.* **27** (1978) 121.
7. A. M. DONALD and E. J. KRAMER, *J. Mater. Sci.* **17** (1982) 1765.
8. A. J. KINLOCH and R. J. YOUNG, in "Fracture Behaviour of Polymers" (Elsevier, Amsterdam, 1988) ch. 5.
9. J. P. DEAR, *J. Mater. Sci.* **26** (1991) 321.
10. J. P. DEAR and J. G. WILLIAMS, *ibid.* **28** (1993) 259.
11. J. M. GREIG and L. EWING, in Proceedings of the 5th International Conference on Plastic Pipes, York, edited by M. J. Littlewood (1982) Paper 13.
12. J. G. WILLIAMS, *Int. J. Fract.* **33** (1987) 47.
13. A. IVANKOVIC and J. G. WILLIAMS, *ibid.* **64** (1993) 251.
14. P. N. R. KEEGSTRA, J. L. HEAD and C. E. TURNER, in Proceeding of the 4th International Conference on Fracture, Waterloo, edited by D. M. R. Taplin (1977) Paper 346.
15. T. NISHIOKA and S. N. ATLURI, *J. Appl. Mech.* **47** (1980) 570.

Received 29 May
and accepted 8 November 2002